IEEE Access
Multidisciplinary : Rapid Review : Open Access Journal

Method for Measuring Rotation Angle of Faucet Handle Based on Machine Vision

Jie Chen, Qian Yuan, Bin Li
School of Mechanical and Electrical Engineering and Automation, Shanghai University, Shanghai, China
Corresponding author: Bin Li (sulibin@shu.edu.cn)

ABSTRACT The faucet's quality inspection is an integral component of the faucet production process. Sensitivity is an essential parameter to be considered in the detection process. In the traditional sensitivity measurement method, the angle of the rotating handle is reflected by the angle of the motor rotation. However, the motor's axis and the faucet's axis are not the same, so the angle measured by the motor is not the angle of the handle. There is a large error through the mechanical transmission structure to drive the handle movement, no matter the adopted transmission method. This paper proposes a faucet rotation angle detection system that uses machine vision to measure the faucet handle's rotation angle. Experiments show that the system's measurement error is less than ±0.5° and meets the system's error requirements for the rotation angle of the faucet handle when the camera's installation height is within a specific range.

INDEX TERMS Faucet handle; measurement system; geometric model; angle recognition; image processing

I. INTRODUCTION

In the processing and production of the faucet [1], the quality detection of the faucet is a very complicated process which occupies a significant position. Furthermore, it is also a key link in quality control. Relevant scholars have analyzed and studied the factors affecting faucets' quality [2]-[3]. The faucet detection equipment is a crucial factor that influences the quality of faucets.

At present, many equipment and methods for detecting faucets have been developed. The French company LF Technologies has invented a constant temperature performance test bench. When the device to be tested is placed on the bench, it will start the faucet according to the pre-programmed test scenario and measure the pressure, flow rate, and temperature. Y. Xu et al. [4] proposed a single-handle dual-control faucet service life test bench to measure a single-handle dual-control faucet's service life. R. P. Monteiro and C. J. A. Bastos-Filho [5] designed an automatic system to help identify defects in sanitary ware. The system deploys a supervised deep learning technique. The trained models presents an average precision superior to 99% and an execution time inferior to 0.018s. A faucet sensitivity detection equipment based on a microcontroller was designed by K. Xin and T. Zhang [6]. The equipment collects temperature, pressure, and flow sensor data through the control of stepping motors, water pumps and cylinders. Then the equipment displays the data on an industrial PC.

Machine vision is to use the images collected by the vision system to obtain the required information and to determine whether the measurement target meets the specifications in the light of prior knowledge [7]. It has the advantages of a high degree of automation, high detection accuracy, non-contact measurement, and high detection efficiency. Due to the rapid development of science and technology, many traditional testing methods have been unable to meet the testing needs or require higher costs. The use of machine vision can solve many problems in industrial image detection links. For example, size detection [8-10], the position detection of products [11], the quality detection of products [12-16], tool detection, contour detection [17], and so on.

Different from detection methods using angle sensors, a new method of detecting the wheel's steering angle based on computer vision was proposed by S. Tian et al. [8]. In this manuscript, the steering direction is determined by analyzing the difference between the wheels' left and right steering. Threshold segmentation and edge extraction methods are used to extract the wheels' contour information and then obtains the wheels' steering angle in the image. In order to improve the accuracy and efficiency of the measurement of porous parts, a high-precision measurement method based on machine vision was proposed by W. Y. Zhang et al. [9]. In this research, the improved cubic spline interpolation algorithm and bilinear interpolation algorithm can locate the boundary more accurately after using the Sobel operator to find the edge roughly. The measurement accuracy of this method can reach sub-pixel level. S. Liu et al. [10] introduced a method for extracting the tubular 3D skeleton of a non-circular section tube based on multi-view vision. Experimental

1

results show that the average deviation does not exceed 0.3 mm, and the measurement time is less than 5 s. T. Tsuji et al. [11] proposed an automatic draft reading method. This method uses morphological operations to detect draught marks and estimates each frame's waterline through Canny edge detection and robust estimation. M. García et al. [12] proposed an image processing and machine learning technology integrated with the Arduino Mega board so as to evaluate and select the best quality green coffee beans. The k-nearest neighbor algorithm is used to determine the quality of coffee beans and the corresponding defect types. Defect detection using machine vision technology plays a vital role in the manufacturing process of mobile phone screen glass (MPSG). C. X. Jian et al. [13] developed an improved MPSG defect recognition system. A contour-based registration (CR) method is used to generate the template image and align the MPSG images. To segment defects with fuzzy gray boundaries from noisy MPSG images, this research developed an improved fuzzy c-means clustering (IFCM) algorithm. A novel anomaly detection method based on Gaussian Restricted Boltzmann Machine (GRBM) was proposed by Y. Zhang et al. [14]. The method integrates the free energy function into the objective process in the two stages of product quality inspection, thereby performing apparent gradient compensation. S. Liang et al. [15] proposed a new concrete crack extraction and classification algorithm based on machine vision. The improved OTSU threshold segmentation method is used to extract cracks in the paper. Combining the fracture skeleton line's extension direction and the gray features of the crack edge can connect the fracture points. J. P. Yun et al. [16] designed a defect inspection system that used a dual lighting structure to distinguish uneven defects and color changes by surface noise. The paper presents an algorithm that consists of a Gabor filter and uses a binarization method to extract the shape of defects. Considering the problem of automatic inspection of industrial metal pieces, J. Marot et al. [17] adapt the level set method for the first time to distinguish hollow regions in metal pieces from the ground surface. The method was compared with the Canny edge enhancement method. Experiments on two industrial images show that the method can correctly extract fuzzy contours and is robust against noise.

In the faucet's quality detection, the sensitivity of the faucet [18] is the crucial parameter. According to EN 817:2008 [19], sensitivity is defined as: when the opening of the faucet handle is the largest (the flow is the largest), the faucet handle is evenly and slowly rotated from the cold water end to the hot water end, and then from the hot water end to the cold water end. Then draw the relationship curve between the mixed water temperature (T) and the displacement or angle (G) of the temperature regulating device as shown in Fig. 1. The two values G1 and G2 between Tm-4 ° C and Tm+4 ° C of the mixed water temperature are obtained according to the drawn curve. The smaller of the two values of G1 and G2 is the sensitivity. T is the water temperature at the faucet outlet, and G is the

displacement or rotation angle of the test equipment. The rotation angle is the angle at which the top of the faucet handle rotates.
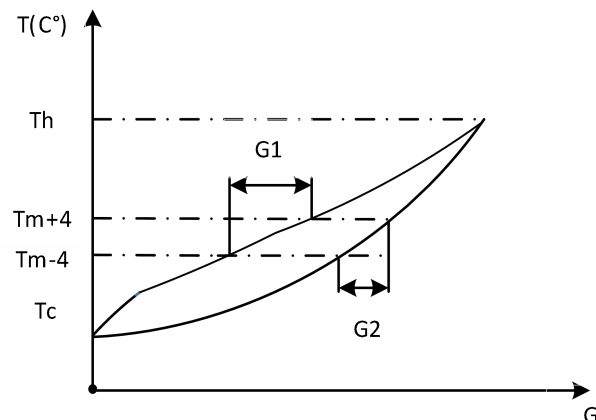

FIGURE 1. The function curve of the mixed water temperature (T) and the displacement or rotation angle (G) of the end of the faucet handle.

This work presents a non-contact measurement method for measuring the rotation angle of a single-handle dual-control faucet. The first step is to explain the principle that the faucet handle's apex's rotation trajectory is a circle. The second step is to analyze the structure of the system and build a geometric model of the system. Then, the reasonable placement range of the camera is deduced according to the constructed geometric model. The third step is to measure the center of the rotation trajectory at the faucet handle's tail. After the camera collects the images of the faucet handle's six positions, it is necessary to preprocess the image. The image preprocessing process contains median filtering and adaptive uneven illumination algorithm based on two-dimensional gamma function to remove uneven illumination. A moving target detection method that combines the background difference method and the AND operation is subsequently used to extract the handle in each position image. After performing the AND operation with the handle images detected at six positions to obtain the faucet handle's rotation trajectory, the Hough transform is used to detect the center of the rotation trajectory of the faucet handle. The following step is to adjust the center of the circle according to this paper's center adjustment method to make the center of rotation more precise. The fourth step is to recognize the center of the circle circumscribed at the tail of the handle by the Hough transform detection circle algorithm after the pre-processing and moving target detection of each faucet handle's collected images. After obtaining the center coordinates of the handle's rotation trajectory and the center coordinates of the circumscribed circle at the handle's tail, the current rotation angle of the faucet can be calculated.

II. System design

As shown in Fig. 2, the faucet moves from the rightmost end to the leftmost end when the opening of the

faucet handle is the largest in the light of the definition of sensitivity measurement. The straight line passing through the center of the circumscribed circle at the end of the handle and the center of the circumscribed circle at the top of the handle is the central axis ($l_0^{'}$, $l_1^{'}$ ... $l_n^{'}$). The point of intersection of the central axis and the bottom of the faucet handle is the apex of the tail of the handle, and the point of intersection of the central axis and the top of the faucet handle is the apex of the top of the handle. Analyzing the rotation trajectory of the top of the faucet handle and the top of the faucet handle's tail，it can be found that the trajectories of the vertices at both ends are two inverted sectors with the same angle when the faucet handle rotates from the rightmost end to the leftmost end. According to Fig. 2, when the faucet rotates to each position, the center of the handle rotation trajectory is O and the center of the circumscribed circle at the tail of the handle is O01, O02, ... Supposing that the coordinate system is established with point O as the center, the rotation angle of the faucet is θ . The top of the faucet and the tail of the faucet rotate on the strength of the sensitivity's definition at a speed of $0.5°/s$. The rotation angles of the top of the faucet handle, the tail of the faucet and the central axis of the faucet are the same. The rotation angle of the faucet handle should be the rotation angle of the top of the handle according to the definition of sensitivity in EN817:2008. However, in the actual operating device, the top of the handle is clamped by the clamp, which will block a part of the top image of the handle. It will be impossible to collect a complete top image of the handle. On account of the fact that the rotation angles of the top of the handle and the tail of the handle are the same, the tail of the handle which can be collected a complete image is selected for system design and analysis. It can be concluded from Fig. 2 that the rotation angle of the apex of the faucet handle tail is equal to the rotation angle of the line which connects the center of the handle rotation trajectory and the center of the circle circumscribed by the handle tail. According to the coordinate system established in Fig. 2, the angle of the current position of the faucet is represented by the angle of a straight line on the Oxy coordinate system, which connects the center of the rotation trajectory of the tail of the faucet handle and the vertex of the bottom of the faucet handle at the current position.

The system is designed and the structure of the measurement system is shown in Fig. 3. The measurement system is mainly composed of a motor, a clamp, a camera, a faucet to be tested and a computer. The motor is located at the top of the device and its installation position is fixed. The clamp is connected with the motor and drives the faucet handle to rotate. The working process of the system is as follows:
(1)　The motor drives the faucet to rotate at a certain speed.
(2)　The camera collects images.
(3)　The angle measurement program recognizes the angle and outputs the angle information and image
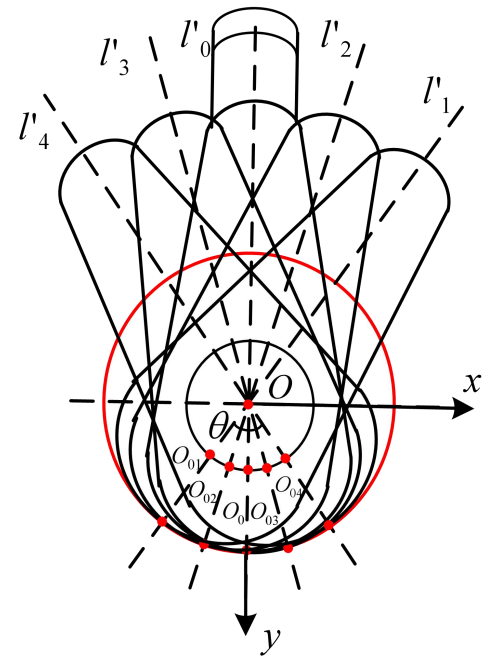
information.

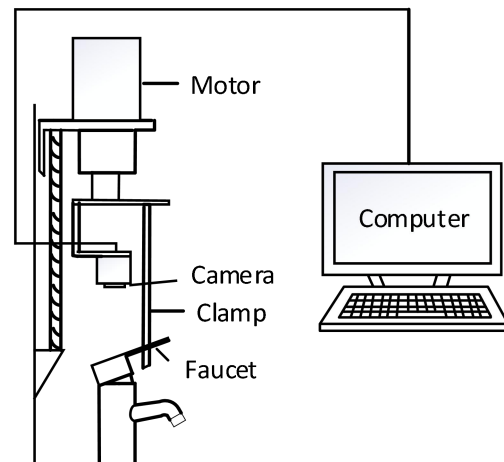**FIGURE 2. Rotation trajectory when the faucet handle is opened at the maximum.**

FIGURE 3. The overall structure of the measurement system.

A.　SYSTEM GEOMETRIC MODEL

As shown in Fig. 4, the geometric model of the system is designed on the basis of systems. Assuming that in the faucet angle measurement system shown in Fig. 4, "Camera" is the camera and O' is the optical center of the lens. The effective field of view that the camera can capture images is represented by O'-ABCD. α_h is the horizontal field of view angle of the camera. α_v is the vertical field of view angle. α_d is the diagonal field of view angle. N_A is the number of pixels in the horizontal direction of the image, and N_B is the number of pixels in the vertical

This article has been accepted for publication in a future issue of this journal, but has not been fully edited. Content may change prior to final publication. Citation information: DOI 10.1109/ACCESS.2020.3034103, IEEE Access

J, Chen *et al*. :Method for Measuring Rotation Angle of Faucet Handle

direction of the image. The point of intersection of the plane ABCD and the optical axis passing through the optical center O' point is O_1. The distance from the optical center to the O_1 point is the installation height H of the camera. l'' represents the faucet handle. l is the projection of the faucet handle on a plane which is parallel to the plane ABCD. A three-dimensional coordinate system is established with point A as the origin, the AB direction as the x' axis, the AD direction as the y' axis, and the direction parallel to the optical axis as the z' axis. After a picture is taken, the image coordinate system is a coordinate system established with C as the origin, CD direction as x'' axis, and CB direction as y'' axis. Regarding the center of rotation O as the origin, the x-direction is parallel to x'' and the y-direction is parallel to y'' to establish a faucet coordinate system named the coordinate system Oxy. The current rotation angle θ and the maximum rotation angle θ' of the faucet handle can be described according to the Oxy coordinate system.
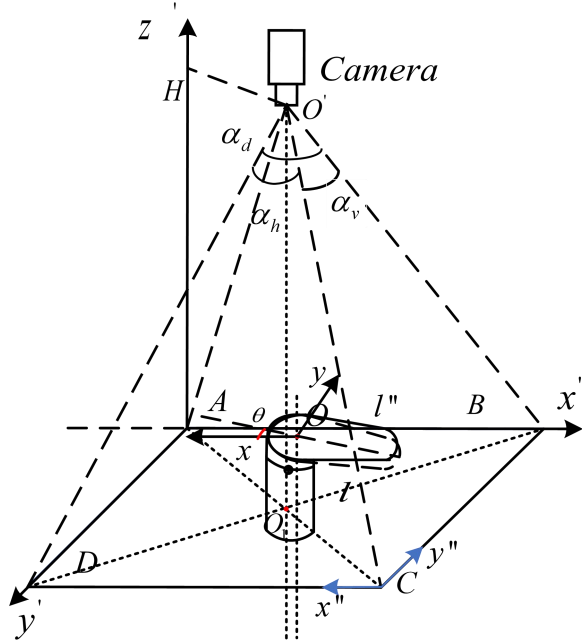

FIGURE 4. System geometry model.

AB and AD can be expressed as:

$$AB = \frac{H}{\cos\frac{\alpha_d}{2}} * \sin\frac{\alpha_h}{2} * 2 \qquad (1)$$

$$AD = \frac{H}{\cos\frac{\alpha_d}{2}} * \sin\frac{\alpha_v}{2} * 2 \qquad (2)$$

B. THE INSTALLATION HEIGHT OF THE CAMERA

As shown in Fig. 5, at present, the handle length L' of the faucet on the market mostly satisfies $L' \leq 120mm$, the

range of opening ϑ mostly satisfies $\vartheta \leq 25°$, and the maximum rotation angle θ' mostly satisfies $\theta' \leq 120°$. This paper only discusses faucets that satisfy $H' \leq 220mm$.

When the opening of the faucet handle is maximum, as shown in Fig. 5, the relationship between ΔH and ϑ is:

$$\Delta H < L' \times \sin\vartheta \qquad (3)$$

The installation height H should satisfy $H > \Delta H + H'$. Take $\vartheta_{max} = 25°$, $H'_{max} = 220mm$, and $L'_{max} = 120mm$, then:

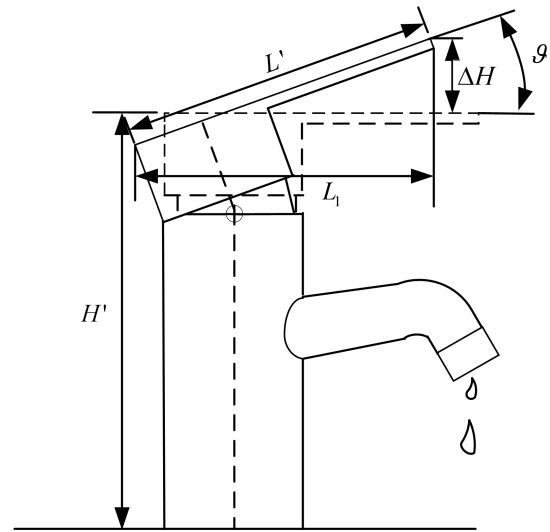$$H \geq \Delta H_{max} + H'_{max} = 270.71 lmm \qquad (4)$$

FIGURE 5. Schematic diagram of faucet handle size.

1) AMINIMUM INSTALLATION HEIGHT

One of the conditions for measuring the faucet handle's rotation angle is that the camera can capture a complete handle image during the entire rotation process. There is always a minimum plane $A_{min}B_{min}C_{min}D_{min}$, which can fully display the images of all positions of the faucet handle during the rotation. At this time, the height of the camera is H_{min}, as shown in Fig. 6. The conditions that H_{min} should satisfy are:

$$H_{min} = \frac{\cos(\frac{\alpha_d}{2})}{2\sin(\frac{\alpha_h}{2})}[2(L'-R)*\cos\vartheta*\cos(90-\frac{\theta'}{2})] \qquad (5)$$

$$H_{min} \geq \frac{L'*\cos\vartheta*\cos(\alpha_d/2)}{2\sin(\alpha_v/2)} \qquad (6)$$
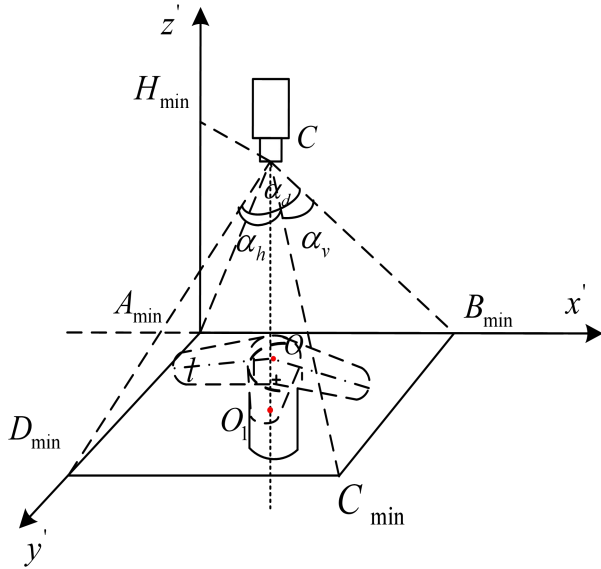
FIGURE 6. Geometric model at the minimum installation height.

R is the radius of the trajectory of the apex of the tail of the faucet when the opening of the faucet handle is the largest, and R<L'. H_{min} gets the maximum value when R=0. According to the parameters in the experiment: $\alpha_d = 80°$, $\alpha_h = 65°$, $\alpha_v = 50°$, $L'_{max} = 120mm$, $\theta'_{max} = 120°$, $\vartheta \leq 25°$. The minimum installation height of the camera should satisfy the following equation:

$$H \geq H_{min} = 134.28mm \qquad (7)$$

2) MAXIMUM INSTALLATION HEIGHT

The central idea of determining the rotation angle of the faucet is to obtain the rotation angle of the central axis of the faucet. It is assumed that the length of the central axis extracted from the image occupies n pixels in the image, and the object rotates around a fixed point. The theoretical detection accuracy is:

$$\Delta\theta = arctg(\frac{1}{n-1}) \qquad (8)$$

In equation(8), $\Delta\theta$ is the detection accuracy and n is the number of pixels occupied by the straight line.

As shown in Fig. 5, L_1 is the linear length of the central axis of the faucet handle. The relationship between L' and L_1 is:

$$L_1 = L'*\cos\vartheta \qquad (9)$$

Supposing that there are n pixels on the straight line L_1, $H_{\Delta\theta}$ is the installation height of the camera when the image detection accuracy is $\Delta\theta$. The following results can be derived from equations (1) and (8):

$$H_{\Delta\theta} = \frac{\cos(\alpha_d / 2)*L_1*N_A*\tan(\Delta\theta)}{2\sin(\alpha_h / 2)*[1+\tan(\Delta\theta)]} \qquad (10)$$

It can be concluded that the smaller $\Delta\theta$ is, the

smaller $H_{\Delta\theta}$ is, and the larger n is. The following data can be obtained from the description of the system equipment: $\Delta\theta_{max} = 0.5°/s$, $L_{1max} = 108.76mm$, $N_A = 640$, $\alpha_d = 80°$, $\alpha_h = 65°$. The relationship between the maximum installation height H_{max} of the camera and the required image detection accuracy $\Delta\theta_{max}$ is:

$$H \leq H_{max} = H_{\Delta\theta_{max}} = 429.28mm \qquad (11)$$

3) THE RELATIONSHIP BETWEEN FOCAL LENGTH AND INSTALLATION HEIGHT

The focal length (f) refers to the distance from the optical center of the lens to the focal point of the light when parallel light is incident. α_d satisfies the following relationship:

$$\alpha_d = 2*\arctan\frac{d}{2f} \qquad (12)$$

In equation (12), d is the diagonal length of the CMOS target surface, and f represents the focal length.

The relationship can be deduced based on the geometric model of the system established in Fig. 4:

$$\frac{\frac{\sqrt{AB^2 + AD^2}}{2}}{H} = \tan\frac{\alpha_d}{2} \qquad (13)$$

From equations (5) and (6), ABmin and ADmin can be derived. ABmin and ADmin can be expressed as:

$$AB_{min} = 2*(L'-R)*\cos\vartheta*\cos(90-\frac{\theta'}{2}) \qquad (14)$$

$$AD_{min} = L'*\cos\vartheta \qquad (15)$$

The parameters in the experiment are: $f = 3.6mm$, $\vartheta \leq 25°$, $\alpha_d = 80°$, $L'_{max} = 120mm$, and $\theta'_{max} = 120°$. H should satisfy:

$$H \geq 129.61mm \qquad (16)$$

The installation height of the actual measuring device reserved for the camera is less than 400mm. According to equations (4), (7), (11) and (16), the available installation height range is:

$$270.71mm \leq H \leq 400.00mm \qquad (17)$$

III. IMAGE PROCESSING

The steps to determine the rotation angle of the faucet handle are:

(1) The first step is to detect the center of the faucet handle tail's rotation trajectory.
(2) The second step is to measure the circumscribed center of the faucet handle tail.
(3) The third step is to calculate the rotation angle of the current faucet handle.

5

## A. CENTER OF ROTATION TRAJECTORY OF THE FAUCET HANDLE TAIL

The measurement process of the center of the rotation trajectory of the faucet handle tail is shown in Fig. 8. Rotating the faucet handle to the rightmost end and then to the leftmost end to collect the images at the rightmost end and the leftmost end. Then a ruler is used to measure the rotation angle to roughly obtain the maximum rotation angle θ' of the faucet. After that, θ' is divide into n' parts. This step aims to reduce the number of processed pictures, and $\theta_v = \dfrac{\theta'}{n'}$. Collecting a picture every θ_v and save it for processing. Finally, the faucet handle in each image is detected, and perform an AND operation between each segmented handle and the previous handle.The contour of the required part is obtained by the Canny edge detection algorithm. The center of the track circle at the tail of the faucet handle is detected by the Hough algorithm.P

The rotation trajectory of the faucet handle tail is a circle with O(A, B) as the center and O(A, B) to the apex of the faucet handle tail as the radius. Based on the theorem of determining a circle with three points, the center of the rotation track of the faucet tail can be measured with only three images. However, in real life, the size of the circumscribed circle at the tail of the faucet handle varies. If the circumscribed circle is too small, it may happen that the circumscribed circles of the three faucet handles do not intersect. But if taking too many pictures of the faucet handle, although the extracted edge is closer to a circle, it will lead to a long processing time. As shown in Fig. 7, it can be seen that the edges of the faucet handles with 5 positions have more points on the rotation trajectory and the shape is closer to a circle. In the actual situation, 5 or more (appropriate number) of faucet handle images can be selected for processing according to the actual situation.
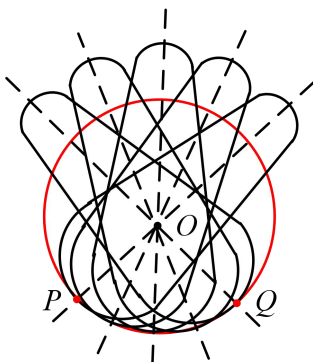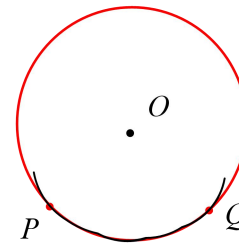
(b)
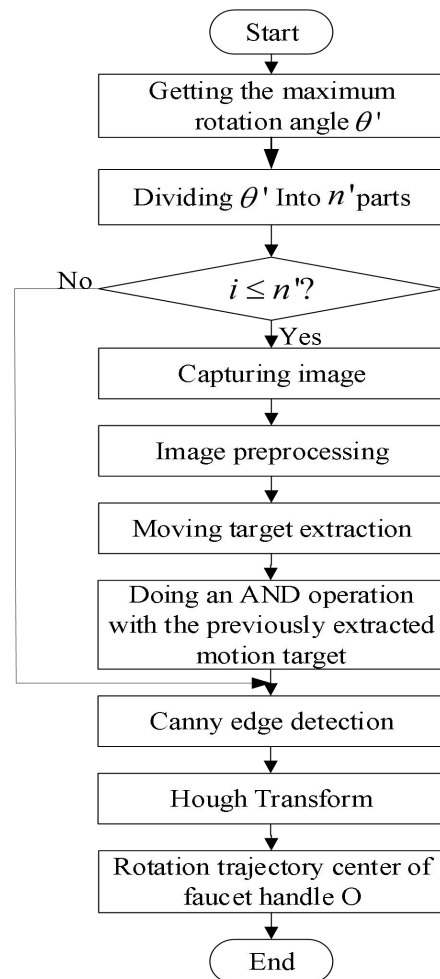
FIGURE 7. Schematic diagram of handle and edge when n=4.

FIGURE 8. Flow chart for determining the center of the trajectory.

(a)

1) IMAGE PREPROCESSING

After the image acquisition is completed, and the image is preprocessed. Since some faucets are made of metal with reflective properties and the experimental device may block the light, the illumination of the collected images is uneven. It will lead to some essential details that cannot be highlighted or even covered. In order to reduce the impact of illumination on the collected images, this paper uses a two-dimensional gamma function-based adaptive image correction algorithm for uneven illumination proposed by Z. C. Liu et al. [20] to process the picture.

Assuming an image is represented by a two-dimensional function f(x,y), the value of f(x,y) is the brightness value of the image at the coordinate (x,y) point. The expression of the illumination-reflection imaging model is:

$$f(x, y) = r(x, y)i(x, y) \qquad (18)$$

Where i (x, y) is the incident light component, r (x, y) is the reflection component on the surface of the object.

The form of the Gaussian function used in this paper is:

$$G(x, y) = \lambda \exp(-\frac{x^2 + y^2}{c^2}) \qquad (19)$$

Where c is the scale factor, λ is the normalization constant to ensure that G(x, y) comforms to the normalization condition.

The estimated value of the illumination component is to convolve the Gaussian function with the original image:

$$I(x, y) = F(x, y)G(x, y) \qquad (20)$$

In equation (15), F(x,y) is the input image and I(x,y) is the estimated illumination component.

The estimated value of the illumination component can be expressed as:

$$I(x, y) = \sum_{i=1}^{N} \omega_i [F(x, y)G_i(x, y)] \qquad (21)$$

In equation (16), I (x, y) is the light component value extracted and weighted by multiple Gaussian functions of different scales at the point (x, y), ω_i is the weight coefficient of the illumination component extracted by the i-th scale Gaussian function, i=1,2...N is the number of scales used.

Supposing that the input image is F(x, y) and the illumination component is I(x, y). A two-dimensional gamma function is constructed, the expression is:

$$O(x, y) = 255(\frac{F(x, y)}{255})^{\gamma} \qquad (22)$$

In equation (17), $\gamma = (1/2)^{(m-I(x,y))/m}$, O(x, y) is the brightness value of the output image after correction, γ is the index value used for brightness enhancement which contains the characteristics of the image's illumination component, and m is the average brightness of the illumination component. As shown in Fig. 9, it is supposed that the initial frame refers to the image used as the background image and the current image is the handle image at a certain moment as an example.

2) MOVING TARGET EXTRACTION METHOD BASED ON THE COMBINATION OF THE BACKGROUND DIFFERENCE METHOD AND THE AND OPERATION

A moving target detection method combining the background difference method and the AND operation is used to extract the handle image at each position after the captured image is preprocessed.

The image difference method is to subtract the corresponding pixel values of two images to weaken the similar part of the image and highlight the changed part of the image. It is defined as:

$$Dif_{im} = f'(x, y) - g'(x, y) = \begin{cases} f'(O') - g'(O_g') \\ f'(B') - g'(B_g') \end{cases} \qquad (23)$$

In equation (18), O' is the foreground area of the image f'(x, y), f'(O') is the pixel value, B' is the background area, and f'(B') is the pixel value. The positions corresponding to O' and B' in $g'(x, y)$ are defined as O_g' and B_g', and the pixel values are defined as $g'(O_g')$ and $g'(B_g')$.
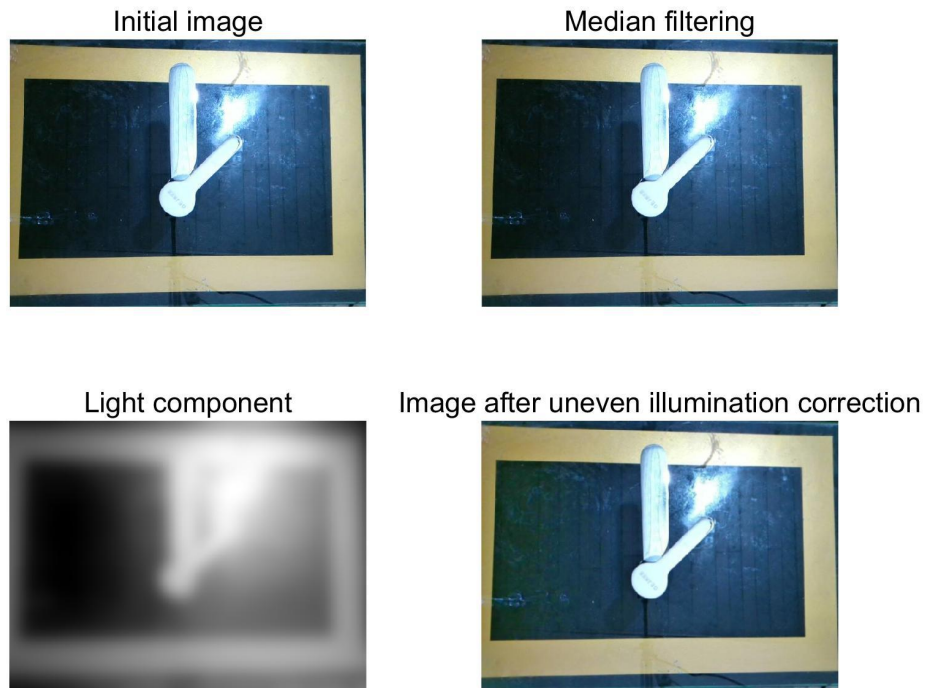
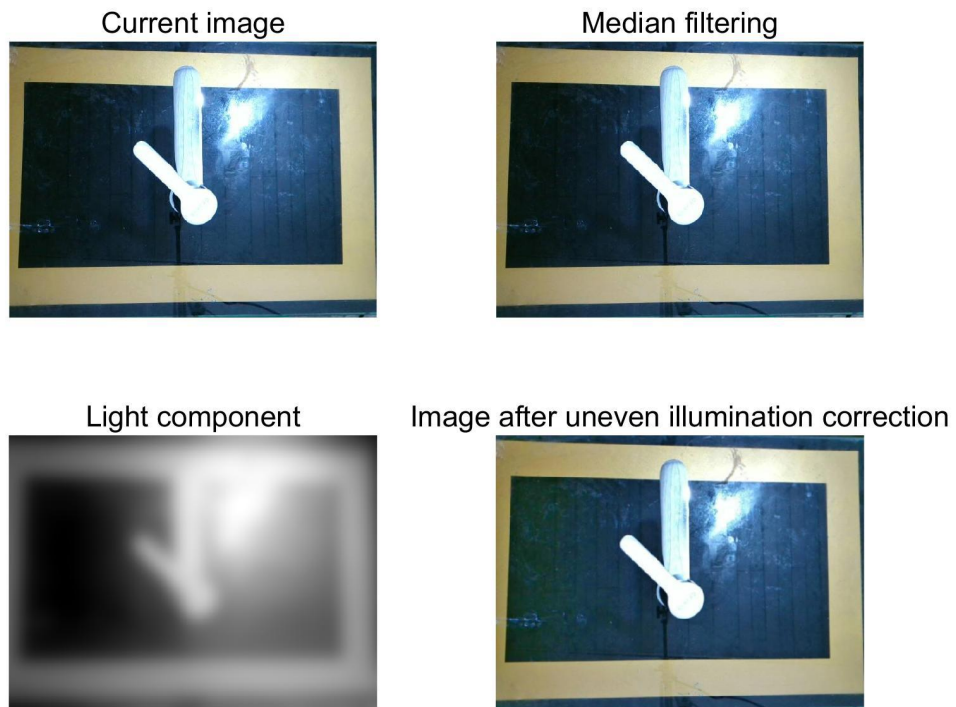**FIGURE 9. The process of weakening the influence of light in the initial image.**

FIGURE 10. The process of weakening the influence of light in the current image.
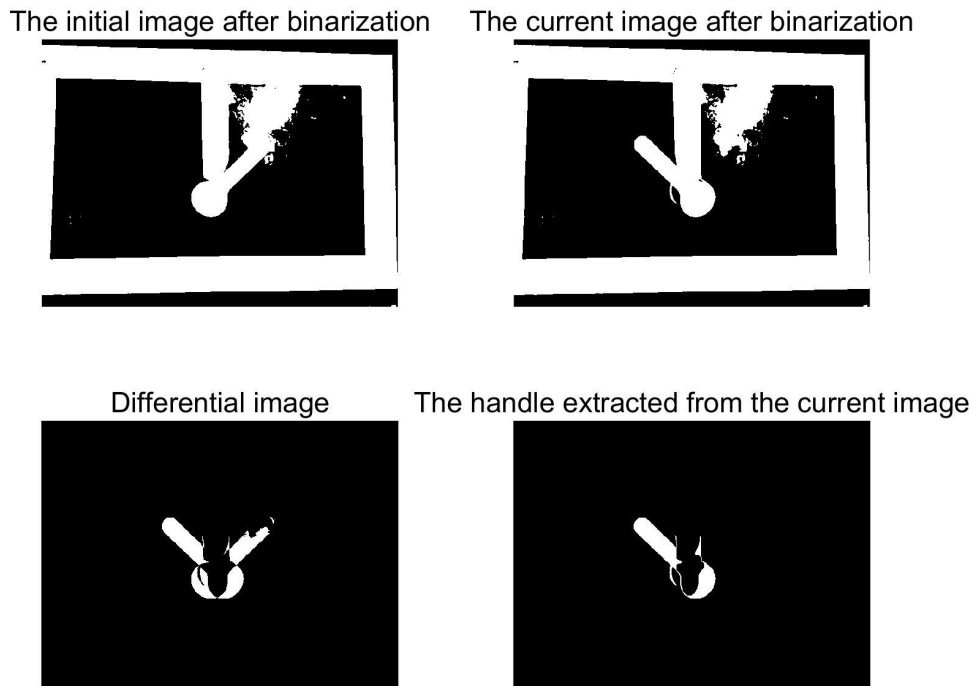
The initial image after binarization   The current image after binarization

Differential image   The handle extracted from the current image

FIGURE 11. The process of extracting the handle.

```
                    ┌─────────┐
                    │  Start  │
                    └────┬────┘
                         ▼
        ┌────────────────────────────────┐
        │   Getting background frame      │
        └────────────────┬───────────────┘
                         ▼
        ┌────────────────────────────────┐
        │      Image preprocessing        │
        └────────────────┬───────────────┘
                         ▼
        ┌────────────────────────────────┐
        │         Binarization            │
        └────────────────┬───────────────┘
                         ▼
        ┌────────────────────────────────┐
        │    Getting the current frame    │
        └────────────────┬───────────────┘
                         ▼
        ┌────────────────────────────────┐
        │      Image preprocessing        │
        └────────────────┬───────────────┘
                         ▼
        ┌────────────────────────────────┐
        │         Binarization            │
        └────────────────┬───────────────┘
                         ▼
        ┌────────────────────────────────┐
        │   Image difference operation    │
        └────────────────────────────────┘
```

Start → Getting background frame → Image preprocessing → Binarization → Getting the current frame → Image preprocessing → Binarization → Image difference operation →

Eliminating small targets → Morphological operations → Internal filling → The differenced image and the current frame after binarization are ANDed → Eliminating small targets → Morphological operations → Extracting the faucet handle in the current image → End
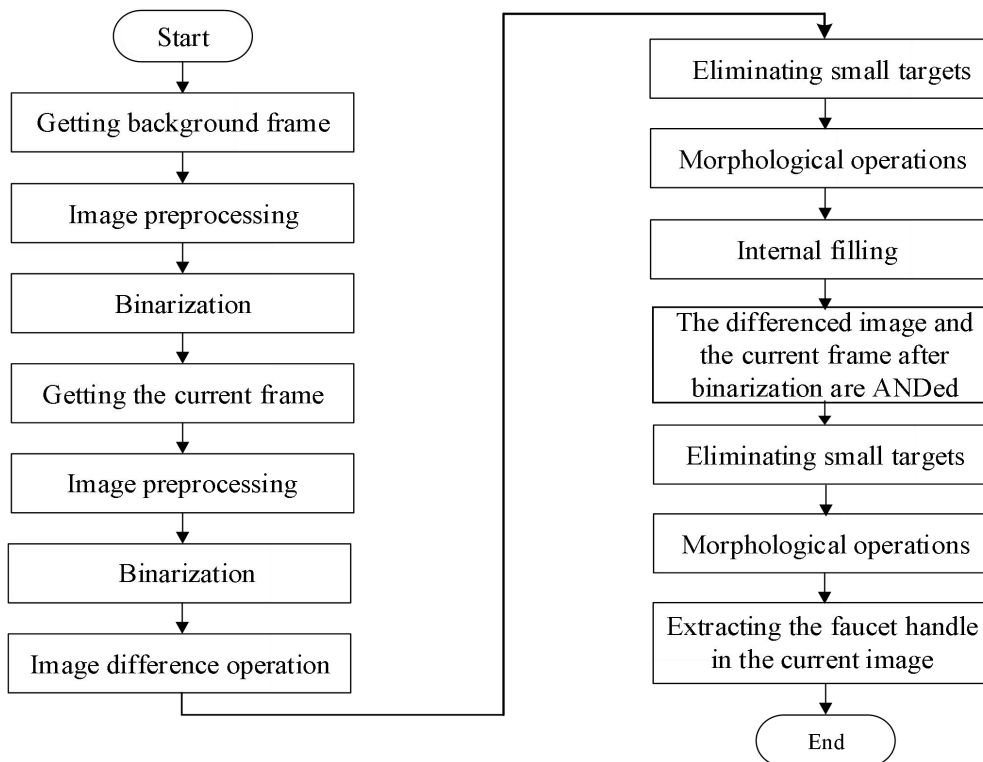
FIGURE 12. Flow chart of extracting handle image.

9

Since the faucet rotates very slowly, some faucet handles cannot extract complete handle image information if the first frame is used as the background. In this paper, the images of the faucet handle rotated to the rightmost end and the leftmost end of the faucet handle are collected in advance and wait for processing. The leftmost image is used as the background when detecting the angle of the faucet handle in the first frame (the rightmost end). When determining the angle of the faucet handle in the last frame (the leftmost end), the rightmost image is used as the background. The θ' of the faucet handle is calculated according to the angle of the rightmost end of the faucet handle and the angle of the leftmost end of the faucet handle. The leftmost image is used as the background when the faucet starts to rotate. The rightmost image of the faucet is used as the background when it is recognized that the rotation angle of the current faucet handle is greater than or equal to half of the obtained maximum rotation angle(θ'). Since the first frame or the last frame is selected as the background, the image extracted by the image difference method includes the handle in the first frame or the handle in the last frame. The faucet handle in the current image can be extracted by performing the AND operation between the differential image and the current handle binarized image. The entire flow chart of extracting moving targets is shown in Fig. 12.

4) ANALYSIS OF USING HOUGH TRANSFORM TO DETECT THE CENTER OF THE ROTATION TRAJECTORY OF THE FAUCET HANDLE

According to the flowchart in Fig. 8, the AND operation is performed on all the extracted handle images, and then the Canny edge detection algorithm is used to detect the edge of the image. The Hough transform is used to extract the center of the circle after obtaining the approximate rotation trajectory of the apex of the tail of the faucet handle.
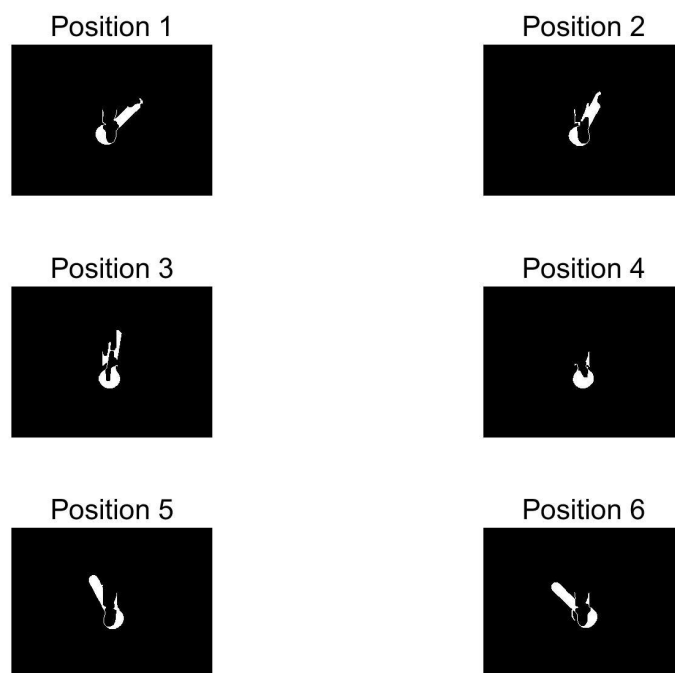

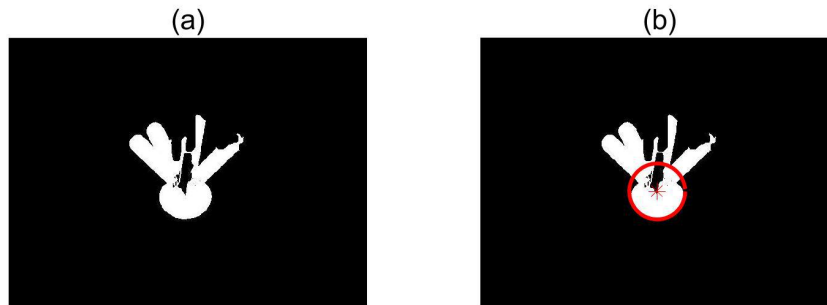**FIGURE 13.** **Handles extracted from images of 6 positions.**

(a) (b)

FIGURE 14. (a) The result of performing the AND operation on all the extracted handle images.

(b) The center of the rotation trajectory of the faucet handle detected by the Hough transform.

B. THE CENTER OF THE CIRCUMSCRIBED CIRCLE AT THE TAIL OF THE FAUCET HANDLE

It can be concluded from Fig. 2 that the angle of the current position of the faucet handle is determined by the center of the rotation trajectory of the tail of the faucet handle and the vertex of the end of the faucet handle. Since the apex of the tail of the faucet handle is difficult to determine and the edges of the extracted faucet handle image may be missing, it will bring errors to the final result. According to the characteristic that the tail shape of the faucet handle is round, the Hough transform is used to fit the tail circle of the handle to fill in the missing edges.

It can be concluded that the apex P at the bottom of the faucet handle, the center O_0 of the circumscribed circle at the bottom of the faucet handle, and the center O of the rotation trajectory of the tail of the faucet handle are in a line from Fig. 15. The current angle of the faucet handle can be represented by the angle of the line connecting the center O_0 of the circumscribed circle at the bottom of the faucet handle and the center O of the rotation trajectory of the tail of the faucet handle in the coordinate system Oxy. The center O_0 of the circumscribed circle at the bottom of the faucet handle is the center detected by the Hough transform.
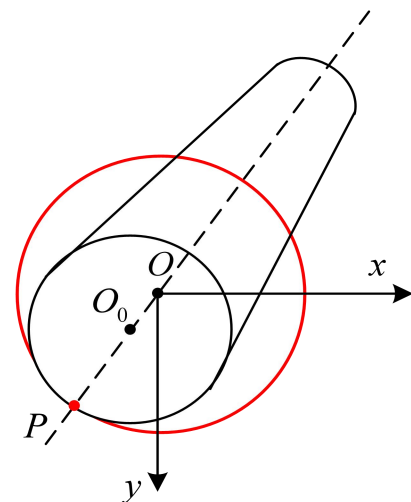
FIGURE 15. Schematic diagram of the relationship between O, P, O_{01}.

Based on the above analysis, the flow chart for measuring the rotation angle can be designed as shown in Fig. 16. After extracting the center of the rotation trajectory of the tail of the faucet handle, the rotation angle of the faucet handle in a certain frame of the image can be recognized. The first step is to collect the current image. The second step is image preprocessing. The third step is to

extract the image of the current handle using the moving target extraction method that combines background subtraction and AND operation. The fourth step is to use the Hough transform to detect the circle center of the circumscribed circle at the tail of the handle. The fifth step is the calculation of the rotation angle.
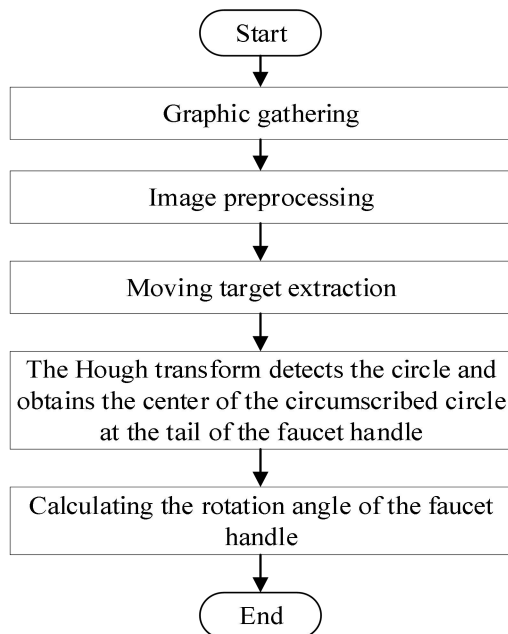
```
        ( Start )
            │
   ┌────────────────────┐
   │  Graphic gathering  │
   └────────────────────┘
            │
   ┌────────────────────┐
   │ Image preprocessing │
   └────────────────────┘
            │
   ┌────────────────────┐
   │ Moving target extraction │
   └────────────────────┘
            │
   ┌──────────────────────────────┐
   │ The Hough transform detects the circle and │
   │ obtains the center of the circumscribed circle │
   │ at the tail of the faucet handle │
   └──────────────────────────────┘
            │
   ┌──────────────────────────────┐
   │ Calculating the rotation angle of the faucet │
   │ handle │
   └──────────────────────────────┘
            │
        ( End )
```
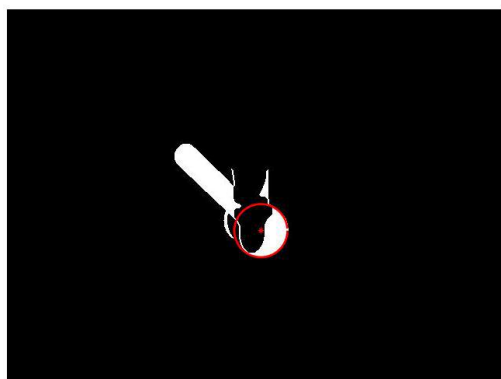
FIGURE 16. Flow chart for determining the rotation angle.

FIGURE 17. The circumcircle of the tail of the handle detected by the Hough transform.

C. ADJUSTMENT OF THE CENTER OF THE ROTATION TRAJECTORY OF THE FAUCET HANDLE

This paper proposes a method to adjust the center of the detected rotation trajectory of the faucet handle tail.

As shown in Fig. 18(a), when the coordinate size of the circle center O is just right, let R_1 represents the

distance from the circle center O to the center of the circle circumscribed by the handle tail when the faucet rotates to the rightmost end and R_2 represents the distance from the circle center O to the center of the circle circumscribed by the handle tail when the faucet rotates to the leftmost end. R_1 and R_2 should have the following relationship:

$$R_1 = R_2 \qquad (24)$$

When $R_1 > R_2$, as shown in Fig. 18(b), it means that the center of the detected rotation trajectory is deviated to the right. The abscissa of the center of the circle needs to bemoved to the left.

When $R_1 < R_2$, as shown in Fig. 18(c), it means that the center of the detected rotation trajectory is deviated to the left. The abscissa of the center of the circle needs to be moved to the right.

When the coordinates of the circle center O are just right, let R_3 represents the distance from the circle center O to the center of the circle circumscribed by the handle tail when the faucet rotates to the middle as shown in Fig. 19(a). R_1 and R_3 should have the following relationship:

$$R_1 = R_3 \qquad (25)$$

When $R_1 < R_3$, as shown in Fig. 19(b), it means that the center of the detected rotation trajectory is deviated upwards. The ordinate of the center of the circle needs to be moved downward.

When $R_1 > R_3$, as shown in Fig. 19(c), it means that the center of the detected rotation trajectory is deviated downward. The ordinate of the center of the circle needs to be moved upward.
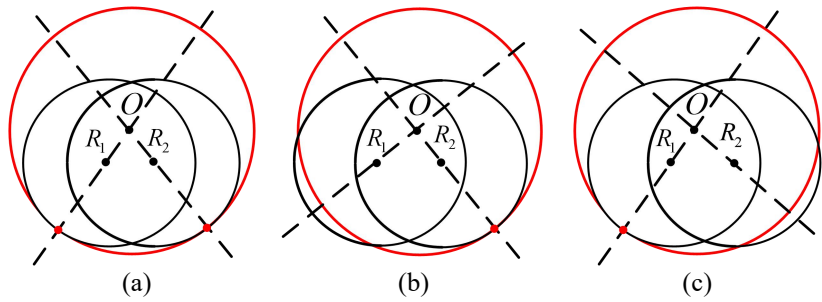
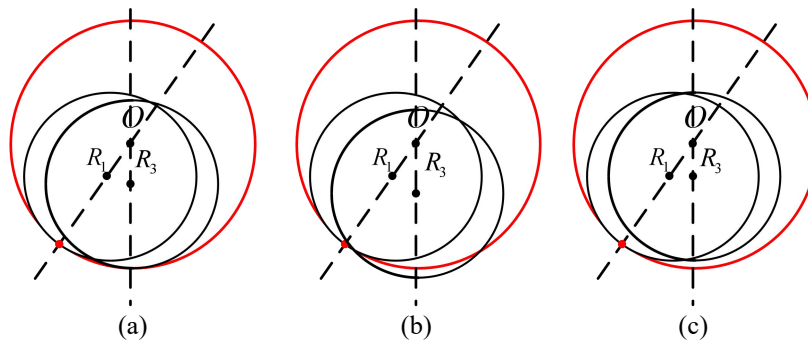**FIGURE 18.** Schematic diagram of the relationship between R_1 and R_2.

FIGURE 19. Schematic diagram of the relationship between R_1 and R_3

D. CALCULATION OF ROTATION ANGLE

After the above steps, two circle centers can be obtained, namely the center coordinates (A, B) of the rotation trajectory of the faucet handle and the center coordinates of the circumscribed circle at the bottom of the faucet handle (a_0, b_0). The coordinate system is established with the upper left corner of the collected image as the origin, the horizontal direction as the x" axis, and the vertical direction as the y" axis according to the system model established in Fig. 4. Comparing the coordinate system established at this time with the coordinate axis Oxy established in the system, it can be concluded that the x-axis is parallel to the x" axis and the y-axis is parallel to the y" axis.
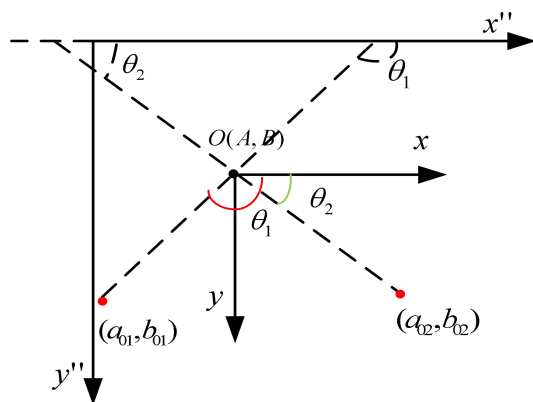

FIEURE 20. Schematic diagram of θ_2 and θ_1 .

(a_{01}, b_{01}) is the center of the circumscribed circle at the end of the faucet handle at the initial position. (a_{02}, b_{02}) is the center of the circumscribed circle at the end of the faucet handle at the current position. The rotation angle θ of the current position of the faucet handle is

$$\theta = \theta_1 - \theta_2 \qquad (26)$$

IV. EXPERIMENTAL ANALYSIS

The experimental device design diagram is shown in Fig. 21 based on the existing experimental conditions. The difference from the measurement system designed in Figure 3 is that there is no motor to drive the rotation and the rotation is manually performed. The method of measuring the rotation angle is to print the picture and measure it with a ruler. Under the existing experimental conditions, there is no motor to hold the faucet handle to rotate, so the experiment is performed by manually rotating the faucet handle. The measurement steps are:

1. When the opening of the faucet handle is the largest, manually rotating the faucet, and measuring the center of the faucet rotation trajectory according to flow chart 7.

2. When the opening of the faucet handle is the largest, manually rotating the faucet and measuring the rotation angle of the faucet at each position according to the flowchart 16.

3. Comparing and analyzing the faucet rotation angle at each position measured manually with the faucet rotation angle measured by the program.
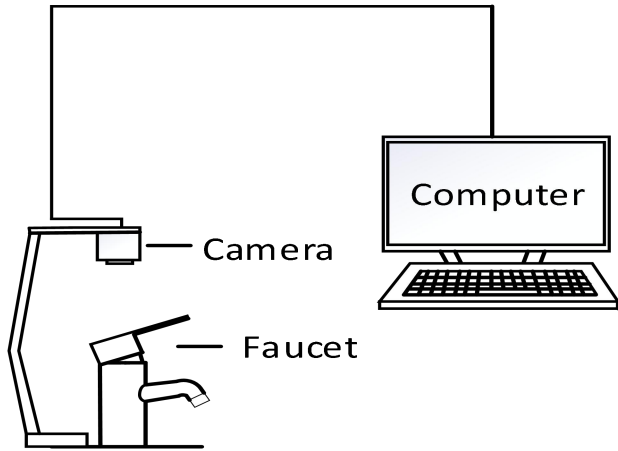
FIGURE 21. **Measurement system under existing experimental conditions.**

In the measurement system under the existing conditions, the specific parameters of the camera used in the measurement are shown in Table 1.

Table 1. **The parameters of the camera used in the measurement system.**

Model		SY8031
Focal length		3.6mm
Resolution		640*480
Field of view	α_d	80°
	α_h	65°
	α_v	50°

In this paper, three different types of faucets are selected for the experiment. The selected faucets are shown in Figure 22. According to the size of the camera installation height range obtained from equation (17), the experimental data of each faucet at the highest camera height, the middle height and the lowest height are recorded. Ideally, the highest height is 400.00mm, the lowest height is 270.31mm, and the middle height is 335.00mm. In the actual operation process, due to the operation of the equipment, the installation height of the three values of the camera cannot fully reach the height shown by the three values, and there is a certain deviation. The faucets' information used is shown in Table 2:

Table 2. **Faucets' size information.**

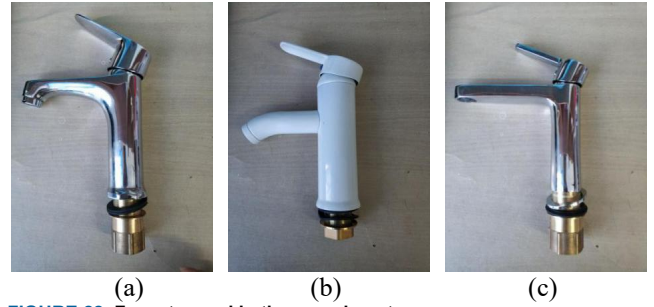|	H'(cm)	$\vartheta(°)$	L'(cm)
Faucet1	18.1	18.3	11.0
Faucet2	16.7	20.1	10.5
Faucet3	15.2	21.1	9.5

FIGURE 22. **Faucets used in the experiment**
(a) faucet1 (b)faucet2 (c)faucet3

In the experiment, the faucets 1, 2 and 3 were placed at different camera installation heights for experiments, and the experimental data was recorded. In the table, O is the center of the rotation trajectory of the faucet handle tail, O_0 is the circumscribed center of the faucet handle tail, O_W represents the center of the circumscribed circle at the end of the handle, θ_1 is the angle of the faucet handle in the first image, θ_2 represents the angle of the current position of the handle measured by MATLAB relative to the image coordinate system, θ represents the rotation angle measured by MATLAB, and θ_c represents the rotation angle measured manually. 'd' can be expressed by θ and θ_c as:

$$d = \theta - \theta_c \tag{27}$$

1. The experimental data of faucet 1 under the camera installation height of 39.5cm, 32.0cm, and 27.1cm.

Table 3. **The initial information of faucet 1 when the camera installation height is 39.5cm.**

H(cm)	The coordinates of point O	The coordinates of point O_0	$\theta_1(°)$
39.5	(305.0, 257.4)	(294.5, 265.5)	142.4

Table 4. **Experimental data of faucet 1 when the camera installation height is 39.5cm.**

$\theta_c(°)$	O_W	$\theta_2(°)$	$\theta(°)$	$d(°)$
10.0	(296.3, 266.9)	132.5	9.9	-0.1
19.5	(298.2, 267.8)	123.2	19.2	-0.3
28.0	(299.6, 269.5)	114.1	28.3	0.3
41.5	(302.4, 270.4)	101.3	41.1	-0.4
49.0	(304.2, 269.7)	93.7	48.7	-0.3
61.0	(306.8, 269.0)	81.2	61.2	0.2
71.4	(309.0, 268.8)	70.7	71.7	0.3
80.5	(310.5, 267.5)	61.4	81.0	0.5
90.4	(312.1, 266.6)	52.3	90.1	-0.3
99.5	(314.6, 266.2)	42.5	99.9	0.4

Table 5. **The initial information of faucet 1 when the camera installation height is 32.0cm.**

H(cm)	The coordinates of point O	The coordinates of point O_0	$\theta_1(°)$
32.0	(307.5, 301.8)	(292.6, 311.9)	145.9

Table 6. Experimental data of faucet 1 when the camera installation height is 32.0cm.

θ_c (°)	O_W	θ_2 (°)	θ (°)	d (°)
12.0	(294.5, 315.2)	134.1	11.8	-0.2
19.8	(297.2, 315.8)	126.3	19.6	-0.2
32.0	(300.8, 317.1)	113.6	32.3	0.3
43.0	(303.8, 317.7)	103.1	42.8	-0.2
53.0	(306.7, 318.9)	92.7	53.2	0.2
60.5	(308.9, 318.7)	85.3	60.6	0.1
70.0	(311.6, 318.5)	76.2	69.7	-0.3
80.5	(314.8, 317.6)	65.2	80.7	0.2
87.0	(316.7, 316.9)	58.6	87.3	0.3
99.5	(320.3, 315.3)	46.5	99.4	-0.1

Table 7. The initial information of faucet 1 when the camera installation height is 27.1cm.

H(cm)	The coordinates of point O	The coordinates of point O_0	θ_1 (°)
27.1	(315.9, 307.3)	(304.4, 320.3)	131.5

Table 8. Experimental data of faucet 1 when the camera installation height is 27.1cm.

θ_c (°)	O_W	θ_2 (°)	θ (°)	d (°)
9.6	(307.6, 322.5)	118.6	12.9	3.3
20.1	(311.1, 323.4)	106.6	24.9	4.8
31.6	(314.5, 324.0)	94.8	36.7	5.1
40.1	(314.7, 322.8)	94.4	37.1	-3.0
49.6	(316.3, 322.6)	88.5	43.0	-6.6
62.6	(320.2. 323.0)	74.7	56.8	-5.8
70.1	(322.8, 322.3)	65.3	66.2	-3.9
77.6	(324.2, 321.4)	59.5	72.0	-5.6
87.6	(327.1, 322.8)	54.1	77.4	-10.2
97.6	(327.9, 321.1)	49.0	82.5	-15.1

2. The experimental data of faucet 2 under the camera installation height of 39.8cm, 34.2cm, and 27.3cm.

Table 9. The initial information of faucet 2 when the camera installation height is 39.8cm.

H(cm)	The coordinates of point O	The coordinates of point O_0	θ_1 (°)
39.8	(313.6, 294.5)	(299.8, 304.8)	143.3

Table 10. Experimental data of faucet 2 when the camera installation height is 39.8cm.

θ_c (°)	O_W	θ_2 (°)	θ (°)	d (°)
9.0	(302.8, 305.7)	134.0	9.3	0.3
18.0	(304.5, 307.4)	125.2	18.1	0.1
30.0	(306.7, 310.3)	113.6	29.7	-0.3
40.5	(309.8, 310.6)	103.3	40.0	-0.5
48.5	(312.3, 311.1)	94.5	48.8	0.3
59.5	(315.5, 311.0)	83.4	59.9	0.4
71.3	(318.8, 310.1)	71.6	71.7	0.4
80.0	(321.2, 309.5)	63.1	80.2	0.2
89.2	(323.2, 307.6)	53.8	89.5	0.3
99.0	(325.3, 306.1)	44.8	98.5	-0.5

Table 11. The initial information of faucet 2 when the camera installation height is 34.2cm.

H(cm)	The coordinates of point O	The coordinates of point O_0	θ_1 (°)
34.2	(327.3, 306.0)	(313.2, 315.9)	144.9

Table 12. Experimental data of faucet 2 when the camera installation height is 34.2cm.

θ_c (°)	O_W	θ_2 (°)	θ (°)	d (°)
9.5	(315.0, 318.0)	135.7	9.2	-0.3
18.6	(317.2, 319.9)	126.0	18.9	0.3
29.0	(319.7, 322.0)	115.4	29.5	0.5
40.0	(323.0, 322.6)	104.5	40.4	0.4
49.0	(325.7, 322.7)	95.5	49.4	0.4
61.0	(329.2, 322.7)	83.5	61.4	0.4
71.0	(331.9, 322.5)	74.4	70.5	-0.5
79.0	(334.4, 321.7)	65.7	79.2	0.2
89.0	(337.0, 320.1)	55.5	89.4	0.4
100.0	(339.4, 318.1)	45.0	99.9	-0.1

Table 13. The initial information of faucet 2 when the camera installation height is 27.3cm.

H(cm)	The coordinates of point O	The coordinates of point O_0	θ_1 (°)
27.3	(314.0, 325.0)	(307.4, 332.1)	132.9

Table 14. Experimental data of faucet 2 when the camera installation height is 27.3cm.

θ_c (°)	O_W	θ_2 (°)	θ (°)	d (°)
10.0	(309.3, 334.0)	117.6	15.3	5.3
19.5	(311.0, 334.0)	108.4	24.5	5.0
29.0	(313.0, 334.9)	95.8	37.1	8.1
39.5	(312.1, 334.5)	101.3	31.6	-7.9
41.0	(314.7, 334.6)	85.8	47.1	6.1
62.0	(317.7, 334.4)	68.5	64.4	2.4
71.5	(320.1, 334.3)	56.7	76.2	4.7
81.0	(319.6, 333.7)	57.2	75.7	-5.3
89.0	(319.9, 332.8)	52.9	80.0	-9.0
100.0	(321.5, 332.4)	44.6	88.3	-11.7

3. The experimental data of faucet 3 under the camera installation height of 39.9cm, 32.5cm, and 27.2cm.

Table 15. The initial information of faucet 3 when the camera installation height is 39.9cm.

H(cm)	The coordinates of point O	The coordinates of point O_0	θ_1 (°)
39.9	(315.7, 272.2)	(304.2, 284.2)	133.8

Table 16. Experimental data of faucet 3 when the camera installation height is 39.9cm.

θ_c (°)	O_W	θ_2 (°)	θ (°)	d (°)
9.4	(306.0, 286.3)	124.5	9.3	-0.1
19.4	(308.9, 287.4)	114.1	19.7	0.3
33.4	(312.6, 289.4)	100.2	33.6	0.2
41.2	(314.9, 288.8)	92.8	41.0	-0.2
52.2	(318.0, 288.6)	82.0	51.8	-0.4
60.4	(320.5, 288.1)	73.2	60.6	0.2
71.2	(323.3, 286.6)	62.2	71.6	0.4
80.4	(325.6, 285.6)	53.5	80.3	-0.1
89.4	(327.4, 283.6)	44.3	89.5	0.1

Table 17. The initial information of faucet 3 when the camera installation height is 32.5cm.

H(cm)	The coordinates of point O	The coordinates of point O_0	$\theta_1(°)$
32.5	(316.5, 270.5)	(303.4, 287.0)	128.4

Table 18. Experimental data of faucet 3 when the camera installation height is 32.5cm.

$\theta_c(°)$	O_W	$\theta_2(°)$	$\theta(°)$	$d(°)$
11.6	(306.9, 289.7)	116.6	11.8	0.2
21.9	(310.2, 291.6)	106.6	21.8	-0.1
31.6	(314.1, 292.0)	96.4	32.0	0.4
41.0	(317.6, 292.3)	87.1	41.3	0.3
51.5	(321.7, 292.2)	76.5	51.9	0.4
60.5	(324.9, 291.5)	68.2	60.2	-0.3
71.5	(329.2, 290.1)	57.1	71.3	-0.2
79.0	(330.8, 287.3)	49.6	78.8	-0.2
89.5	(332.2, 283.3)	39.2	89.2	-0.3

Table 19. The initial information of faucet 3 when the camera installation height is 27.2cm.

H(cm)	The coordinates of point O	The coordinates of point O_0	$\theta_1(°)$
27.2	(340.0, 314.0)	(324.2, 329.9)	134.8

Table 20. Experimental data of faucet 3 when the camera installation height is 27.2cm.

$\theta_c(°)$	O_W	$\theta_2(°)$	$\theta(°)$	$d(°)$
12.0	(327.8, 333.3)	122.3	12.5	0.5
20.0	(330.1, 335.2)	115.0	19.8	-0.2
30.0	(334.3, 335.8)	104.7	30.1	0.1
40.0	(338.0, 335.8)	95.2	39.6	-0.4
50.5	(342.0, 335.5)	84.7	50.1	-0.4
60.5	(345.8, 334.2)	74.0	60.8	0.3
72.4	(350.6, 334.1)	62.2	72.6	0.2
82.0	(353.3, 331.6)	52.9	81.9	-0.1
89.0	(355.4, 329.7)	45.6	89.2	0.2

The error in the experiment comes from:
1. Manually measured angle data will bring certain errors.
2. Errors caused by program algorithms.

Based on the above experimental data, draw a line graph of the d values of faucets 1, 2, and 3 at different heights. Fig. 23 shows the d value of each position of faucet 1 when H=39.5cm, 32.0cm, and H=27.1cm. Fig. 24 shows the d value of each position of the faucet 2 when H=39.8cm, H=34.2cm, and H=27.3cm. Fig. 25 shows the d value of each position of the faucet 3 when H=39.9cm, H=32.5cm and H=27.2cm.
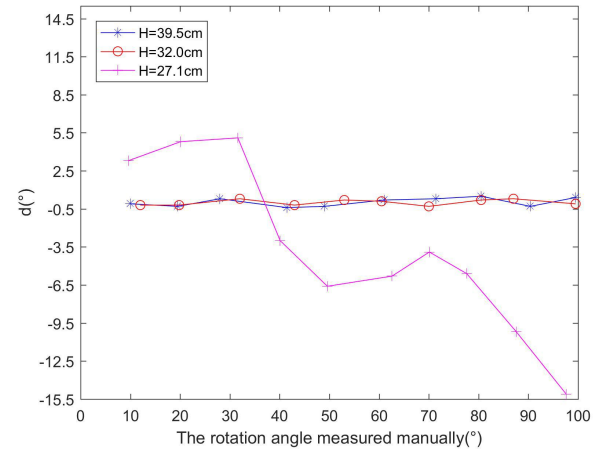

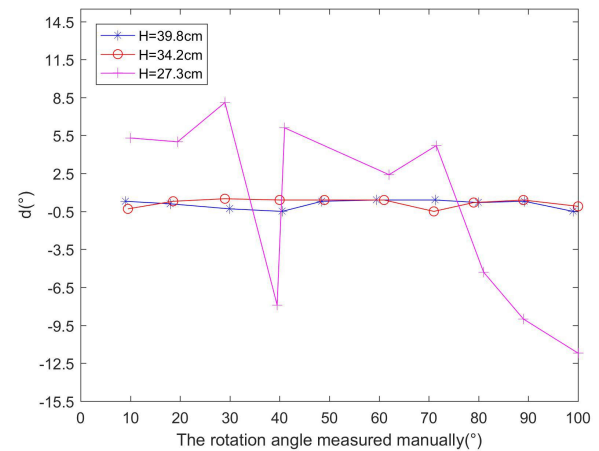**FIGURE 23.** The d value of each position of faucet 1 when H=39.5cm, 32.0cm, and H=27.1cm.

FIGURE 24. The d value of each position of the faucet 2 when H=39.8cm, H=34.2cm, and H=27.3cm.
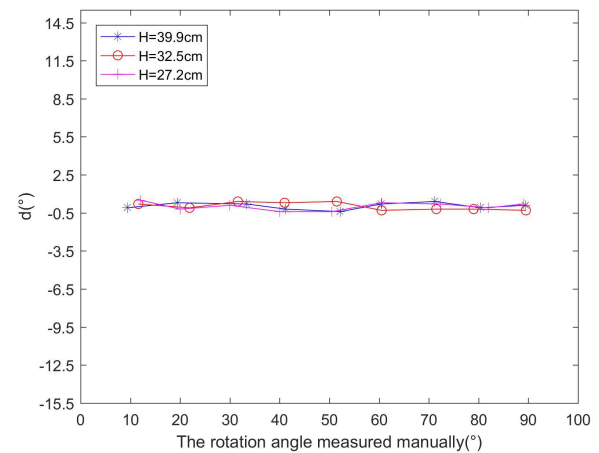

FIGURE 25. The d value of each position of the faucet 3 when H=39.9cm, H=32.5cm and H=27.2cm.

Observing the experimental results, it can be found from Fig. 23 that when the faucet is installed at a height of 39.5cm and 32.0cm, the experimental results meet the accuracy requirements of the system, but the error has deviated from ±0.5° at a height of 27.1cm. Fig. 24 shows that for faucet 2, the experimental results at the height of 39.8cm and 34.2cm meet the accuracy requirements of the system, but the error has deviated from ±0.5° at the height of 27.3cm. From Fig. 25, it can be comclude that for the faucet 3, the accuracy requirements of the system are met at the three heights. The reason for this result is that the length and width of the handles of faucet 1 and faucet 2 are large. When images are collected at the lowest height, the tail of the handle will be distorted in the image. As shown in Fig. 26, when the faucet 1 and the faucet 2 are at the lowest installation height of the camera, the detected center of the circumscribed circle at the tail of the faucet handle is too far from the center axis of the handle. The center coordinate of the circumscribed circle at the end of the handle also affects the adjustment of the center coordinate of the rotation trajectory.
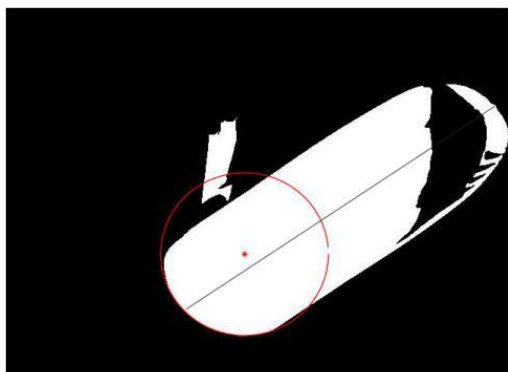

FIGURE 26. The image of the handle at the lowest height of the faucet 1.

Based on the above analysis, when the camera installation height is too low, it will affect the detection accuracy of the system. According to the experimental results, it is more appropriate to limit the installation height to between 32~40cm. Within this height, the detection accuracy of the system is satisfied.

V. SUMMARY

This paper presents a non-contact measurement method for measuring the rotation angle of a single-handle dual-control faucet. The running experiments show that the hardware structure of the system is simple and has great theoretical and practical value. Compared with the traditional method of using a motor to measure the rotation angle of the faucet handle, the measurement method proposed in this paper has the following advantages:

(1) First, within a certain camera installation height range, the measurement system and detection algorithm meet the accuracy requirements of the measurement system.

(2) Second, the rotation angle of the traditional faucet handle is measured by a motor. However, due to the influence of human factors on the installation position of the motor and the faucet, the shaft of the motor and the axis passing through the center of the faucet rotation trajectory are not in line, which affects the accuracy and repeatability of the detection. A method based on machine vision can solve this problem.

(3) Finally, it saves testing costs and increases economic benefits. Compared with a stepper motor, a higher-precision stepper motor costs a lot, and the use of machine vision methods saves detection costs.

REFERENCES

1. W. A. Denham, C. J. Lagarelli, and R. J. Viegener, "Ceramic disc faucet valve," U.S. Patent No. 4 651 770, Mar. 24, 1987.
2. Y. H. Wen, Z. X. He, and Y. K. Huang, "Comparative study on object quality of ceramic sealing faucets," *China Building Materials Technology*, vol. 27, no. 1, pp. 49-55, 2018.
3. R. J, "Chen. Electroplating Quality Problem of Ceramic Cartridge Faucets and Solutions," *Plating and environmental protection*, vol. 33, no. 4, pp.7-9, 2013.
4. Y. Xu, W. Y. Xu, X. D. Dai, Z. Y. Shi, C. P. Shen, & B. Wang, et al. "Service life test stand of single-handle double-control water nozzle," CN201297978Y, September 26, 2008.
5. R. P. Monteiro and C. J. A. Bastos-Filho, "Detecting Defects in Sanitary Wares Using Deep Learning," in *2019 IEEE Latin American Conference on Computational Intelligence (LA-CCI)*, Guayaquil, Ecuador, 2019, pp. 1-6.
6. K. Xin, and T. Zhang.(2019, December). Mechanical structure design of a ceramic sheet sealing nozzle sensitivity test equipment. AIP Conference Proceedings. Available:https://aip.scitation.org/doi/abs/10.1063/1.5137882#.
7. M. Jin, "Measurement method of screw thread geometric error based on machine vision," *Measurement & Control Journal of the Institute of Measurement & Control*, vol. 51, no. 7-8, pp. 304-310, 2018.
8. S. Tian, Y. Zheng, and Z. Shi, "Image processing-based wheel steer angle detection," *Journal of Electronic Imaging*, vol. 22, no. 4, 2013, Art. no. 043005.
9. W. Y. Zhang, X. J. Liu and M. Zhang, "Research on the size measurement of porous parts based on machine vision," in *2017 12th IEEE Conference on Industrial Electronics and Applications(ICIEA)*, Siem Reap, 2017, pp. 242-247.
10. S. Liu et al., "A Universal, Rapid and Accurate Measurement for Bend Tubes Based on Multi-View Vision," *IEEE Access*, vol. 7, pp. 78758-78771, 2019.
11. T. Tsuji , H. Yoshida , and Y. Iiguni, "Automatic draft reading based on image processing," *Optical Engineering*, vol. 55, no. 10, 2016, Art.no. 104104.
12. M. García, J. E. Candelo-Becerra, and F. E. Hoyos, "Quality and Defect Inspection of Green Coffee Beans Using a Computer Vision System," *Applied Sciences*, vol. 9, no. 19, 2019, Art. no. 4195.
13. C. X. Jian, J. Gao, and Y. H. Ao, "Automatic surface defect detection for mobile phone screen glass based on machine vision," *Applied Soft Computing*, vol. 52, pp. 348-358, 2017.
14. Y. Zhang, P. Peng, C. Liu and H. Zhang, "Anomaly Detection for Industry Product Quality Inspection based on Gaussian Restricted Boltzmann Machine," in *2019 IEEE International Conference on Systems, Man and Cybernetics (SMC)*, Bari, Italy, 2019, pp. 1-6.
15. S. Liang, X. Jianchun and Z. Xun, "An Extraction and Classification Algorithm for Concrete Cracks Based on Machine Vision," *IEEE Access*, vol. 6, pp. 45051-45061, 2018.
16. J. P. Yun, et al. "Vision-based surface defect inspection for thick steel plates," *Optical Engineering*, vol. 56, no. 5, 2017, Art. no. 053108.
17. J. Marot et al. "Contour Detection for Industrial Image Processing by Means of Level Set Methods," in *International Conference on Advanced Concepts for Intelligent Vision Systems*. Springer, Berlin, Heidelberg, 2008, pp. 655-663.
18. G. Zhao, C. Y. Lin, J. J. Shao, et al. "Study on the sensitivity of

This article has been accepted for publication in a future issue of this journal, but has not been fully edited. Content may change prior to final publication. Citation information: DOI
10.1109/ACCESS.2020.3034103, IEEE Access

IEEE *Access*

J, Chen *et al*. :Method for Measuring Rotation Angle of Faucet Handle

ceramic sheet sealing faucet," *Ceramics*, vol. 399, no. 1, pp. 39-43, 2019.

19. Sanitary tapware - Mechanical mixing valves (PN 10) - General technical specifications, EN 817-2008, 2008.

20. Z. C. Liu, D. W. Wang. Y. Liu, and X. J. Liu, "Adaptive correction algorithm for uneven illumination image based on two-dimensional gamma function," *Journal of Beijing Institute of Technology*, vol. 36, no. 2, pp. 191-196, 2016.

JIE CHEN received the B.S. degree in automatic control, the M.S. degree in detection technology and automatic equipment, and the Ph.D. degree in control theory and control engineering from Shanghai University, Shanghai, China, in 2002, 2005, and 2010, respectively. She is currently a Lecturer with the School of Mechanical and Electrical Engineering and Automation, Shanghai University. She has authored or coauthored over 31 articles in journals and conferences. Her current research interests include electromagnetic flowmeters and sparse signal processing.
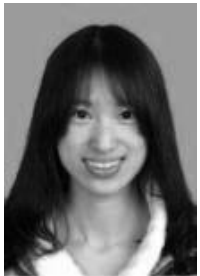
QIAN YUAN received the B.S. degree in electrical engineering and automation from Shanghai University in Shanghai, China in 2013. Currently studying for a master's degree. Her current research interest is machine vision.

BIN LI received the B.S. degree in computer science and the M.S. degree in automation from the Shanghai University of Science and Technology, Shanghai, China, in 1982 and 1988, respectively. He is currently a Professor with the School of Mechanical and Electrical Engineering and Automation, Shanghai University, Shanghai. He has authored or coauthored over 17 refereed articles. He holds 19 patents. His current research interests include electromagnetic flowmeters, vortex flowmeters, ultrasonic flowmeters, sparse signal processing, and calibration instruments.